1. **Preferential uptake of SARS-CoV-2 by pericytes potentiates vascular damage and**

2. **permeability in an organoid model of the microvasculature**

3.

4. Abdullah O. Khan*^[1], Jasmeet S. Reyat[1]^, Harriet Hill[2], Joshua H. Bourne[1], Martina

5. Colicchia[1], Maddy L. Newby[3], Joel D. Allen[3], Max Crispin[3], Esther Youd[4], Paul G. Murray[2;5],

6. Graham Taylor[2], Zania Stamataki[2], Alex G. Richter[2], Adam F. Cunningham[2], Matthew

7. Pugh[2], Julie Rayes*[1].

8.

9. 1. Institute of Cardiovascular Sciences, College of Medical and Dental Sciences, University

10.   of Birmingham, Vincent Drive, B15 2TT, Birmingham, U.K.

11. 2. Institute of Immunology and Immunotherapy, University of Birmingham, Birmingham, B15

12. 2TT, U.K.

13. 3. School of Biological Sciences, University of Southampton, Southampton SO17 1BJ, U.K.

14. 4. Forensic Medicine and Science, University of Glasgow, Glasgow, UK

15. 5. Health Research Institute, University of Limerick, Limerick, Ireland

16.

17. *Correspondence to j.rayes@bham.ac.uk and a.khan.4@bham.ac.uk. ^These authors have

18. contributed equally.

19.

1 **Abstract:**

2 **Aims:** Thrombotic complications and vasculopathy have been extensively associated with

3 severe COVID-19 infection, however the mechanisms inducing endotheliitis and the

4 disruption of endothelial integrity in the microcirculation are poorly understood. We

5 hypothesized that within the vessel wall, pericytes preferentially take up viral particles and

6 mediate the subsequent loss of vascular integrity.

7 **Methods and Results:** Immunofluorescence of post-mortem patient sections were used to

8 assess pathophysiological aspects of COVID19 infection. The effects of COVID-19 on the

9 microvasculature were assessed using a vascular organoid model exposed to live viral

10 particles or recombinant viral antigens. We find increased expression of the viral entry

11 receptor ACE2 on pericytes when compared to vascular endothelium, and a reduction in

12 the expression of the junctional protein CD144, as well as increased cell death, upon

13 treatment with both live virus and/or viral antigens. We observe a dysregulation of genes

14 implicated in vascular permeability including NOTCH3, angiopoietin-2 and TEK. Activation

15 of vascular organoids with IL-1β did not have an additive effect on vascular permeability.

16 Spike antigen was detected in some patients' lung pericytes, which was associated with a

17 decrease in CD144 expression and increased platelet recruitment and VWF deposition in

18 the capillaries of these patients, with thrombi in large vessels rich in VWF and fibrin.

19 **Conclusions:** Together our data indicates that direct viral exposure to the microvasculature

20 modelled by organoid infection and viral antigen treatment result in pericyte infection,

21 detachment, damage and cell death, disrupting pericyte-endothelial cell crosstalk and

22 increasing microvascular endothelial permeability, which can promote thrombotic and

23 bleeding complications in the microcirculation.

24 **Translational Perspective:** Endotheliitis is a serious complication of severe COVID-19

25 patients which remains poorly understood. We identify a pericyte mediated mechanism by

26 which the vasculature becomes compromised, contributing to thrombotic complications,

27 highlighting important avenues for the development of therapies.

1
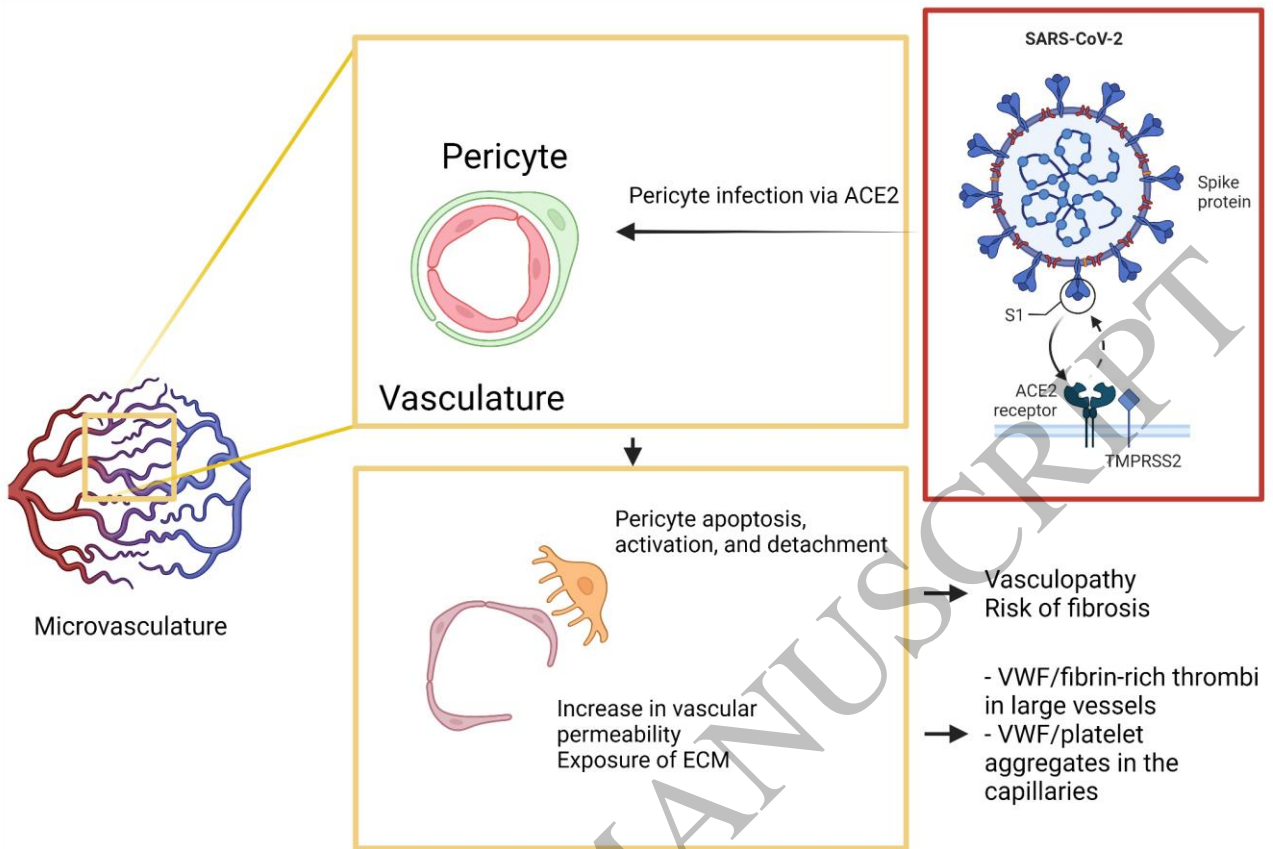
2 **Graphical Abstract**

3

1 **Introduction**

2 Severe acute respiratory syndrome coronavirus 2 (SARS-CoV-2)-associated vasculopathy

3 and endotheliitis are commonly observed in patients with severe COVID-19 [1]. The

4 incidence of macrovascular thrombosis is relatively high in these patients, with arterial

5 thrombosis and venous thromboembolism observed in over 30% of patients [2]. Endothelial

6 activation and injury, disruption of cell membrane integrity, intussusceptive angiogenesis,

7 and widespread microthrombi in alveolar capillaries have also been detected in lung

8 autopsies [3-5]. Under basal conditions, microvascular endothelial cells (ECs) are tightly

9 associated with specialized mural cells (pericytes) that act as integral anchors supporting

10 endothelial vascular integrity and permeability [6]. Infection and subsequent cell damage

11 induce mural cell activation and apoptosis, driving inflammation and disrupting interactions

12 between pericytes and ECs, increasing vessel instability, vascular permeability and

13 potentially driving thrombosis and bleeding [7]. Whether SARS-CoV-2 directly infects

14 endothelial cells and contributes to cell damage and activation remains controversial [8,9,10],

15 with increasing evidence supporting key roles for the stroma, as well as innate immune cell

16 and platelet activation in endotheliopathy [11,12]. Despite the prevalence of these pathologies,

17 the mechanisms driving SARS-CoV-2-mediated endotheliitis and thrombosis both in large

18 vessels and in capillaries remains poorly understood [5,13,14].

19 Following SARS-CoV-2 infection, binding of the viral spike glycoprotein to the host

20 angiotensin-converting enzyme 2 (ACE2) promotes cellular entry, with different proteolytic

21 reactions mediated by Transmembrane Serine Protease 2 (TMPRSS2) and co-receptors

22 required for efficient virion infection [15,16]. Infection-mediated disruption of the epithelial

23 barrier allows the virus to infect the vessel wall, with the efficiency of infection being

24 regulated by ACE2 and its co-receptors expression. ACE2 expression on human

25 endothelium has been shown to be insufficient for viral replication and endothelial activation

26 [8]. Furthermore, inoculation of primary lung endothelial cells with SARS-CoV-2 results in

27 limited infection rates [17,18], while spike pseudovirus can induce mitochondrial damage in

28 endothelial cells [10]. In the absence of clear evidence showing endothelial infection by

29 SARS-CoV-2, other cellular constituents of the vessel wall, such as pericytes, have

30 emerged as potential target cells and sites of infection [19-23]. Indeed, ACE2 expression on

31 brain and cardiac pericytes has been shown to support SARS-CoV-2 infection [22,23].

32 Conversely, lung pericyte infection by SARS-CoV-2 and its effect on endothelial cell

1 activation and integrity in particular, is not well studied [20-24]. This is at least partially due to

2 the difficulty in modelling pericytes environment *in vitro*, a technical challenge which has

3 been addressed in recent years with the development of organoid models. Indeed,

4 microvascular healthy pericytes express ACE2 [15, 25, 26] and this expression can be further

5 increased in pathological conditions such as lung fibrosis [27], a clinical complication

6 observed in patient cohorts known to be vulnerable to COVID-19 infection[28]. The ability of

7 SARS-CoV-2 to infect target cells is heavily dependent on the restricted expression of

8 ACE2, TMPRSS2 and novel proteases and cofactors [19, 26]. Using vascular and kidney

9 organoid models, *Monteil et al* showed that SARS-CoV-2 can directly infect vascular

10 organoids, which can be reversed by human recombinant soluble ACE-2 [29]. However, the

11 cell type involved in SARS-CoV-2 uptake and its effect on vessel wall cell activation and

12 survival is not known.

13 In this study, we assessed the presence of the viral spike glycoprotein in pericytes in lung

14 autopsies from eight patients with COVID-19. We reasoned that direct infection of pericytes

15 with SARS-CoV-2 drives endothelial dysfunction and potentiates thrombotic complications

16 in the microcirculation. We show a heterogenous presence of the spike glycoprotein in lung

17 microvascular pericytes, in particular in patients with documented microvascular and

18 macrovascular thrombosis. Infection of 3D vascular organoids mimicking the

19 microvasculature with SARS-CoV-2, spike glycoprotein and nucleocapsid protein induced

20 pericyte and endothelial death and altered endothelial permeability, independently of

21 endothelial activation. We observed a preferential uptake of SARS-CoV-2 by pericytes

22 associated with a dysregulation of genes regulating endothelial permeability such as

23 NOTCH3 and angiopoietin-2. Our data suggest that pericytes are a critical site of SARS-

24 CoV-2 infection and disruption of pericyte-endothelial interactions promotes thrombosis.

25 **Materials and Methods**

26 **Ethical approvals**

27 Collection of post-mortem FFPE tissue was approved (IRAS: 197937) for tissue obtained

28 via prospective consent post-mortem and retrospective acquisition of tissue in which

29 consent for use in research had already been obtained. Ethics for patient tissue were

30 approved by the Health Research Authority (HRA) with an NHS (National Health Service)

31 REC (Research Ethics Committee); approval issued by North East- Newcastle and North

32 Tyneside 1 (19/NE/0336). All necessary patient/participant written consent has been

1 obtained and the appropriate institutional forms have been archived. This research adheres

2 to the tenets of the Declaration of Helsinki.

3 **Patients**

4 *Post mortem* formalin-fixed and paraffin-embedded lung sections from eight COVID-19, one

5 MERS-CoV, one rhinovirus and two control (non-respiratory-associated diseases) patients.

6 COVID-19 samples were from pre-hospital and hospital deceased patients, with time from

7 symptoms to death ranging from 0-36 days, and ages ranging from 59-89 years old.

8 Patients were not on mechanical ventilation and all had comorbidities (highlighted in

9 Supplementary Table 1).

10 **iPSC culture and organoid generation**

11 Human induced pluripotent stem cells were obtained from Gibco (Thermo) and cultured on

12 GelTrex (Thermo) coated 6-well plates in StemFlex medium (Thermo). Cells were

13 passaged using an EDTA dissociation method, and routinely karyotyped as described [30].

14 Vascular organoid generation was performed in a manner similar to that previously

15 described [31]. Briefly, cells were dissociated and re-plated on Ultra Low Attachment 6-well

16 plates (Corning) in StemFlex supplemented with RevitaCell (Thermo) overnight before

17 commencement of differentiation protocol. On day 0 (d0), cells were collected from Ultra

18 Low Attachment plates and spun down at 500xg before resuspension in Phase I media,

19 which was comprised of APEL2 (Stem Cell Technologies) media supplemented with

20 CHIR90921 (12 µM), and BMP4 (Thermo), FGF2, and VEGFA at 50 ng/ml (Stem Cell

21 Technologies). Cells were incubated at 37 °C and 5 % CO_2 for 3 days, before pelleting by

22 gravitation and resuspension in Phase II medium. Phase II medium was composed of

23 APEL2 medium, VEGFA at 100ng/ml, and FGF2 at 50ng/ml. On day 5 of the protocol,

24 mesodermal blasts were embedded in a mixed matrix hydrogel composed of 60 % Collagen

25 Type I (VitroCol – Advanced Biomatrix) and reduced Growth Factor Matrigel (Corning), and

26 incubated in phase II medium supplemented with 15 % FBS. Fresh media was added on

27 day 8, and sprouted cultures were isolated from the hydrogel at day 10 by scraping and

28 centrifugation. Collected organoids were then cultured individually in 96 well Ultra Low

29 attachment plates (Corning) before treatment at day 15.

30 **Treatment of vascular organoids with SARS-CoV-2 virus or antigens**

31 SARS-CoV-2 England 2 virus (Wuhan) was a kind gift from Christine Bruce, PHE.

32 Recombinant trimeric spike glycoprotein (S) was produced in expressed in human

1   embryonic kidney (HEK) 293F cells as previously described[32]. Nucleocapsid (N) protein

2   was produced in *E.coli* bacteria and purified as described[33]. The levels of endotoxin in the N

3   protein preparation was lower than 0.005 EU/µg. Vascular organoids were treated for 48 h

4   with SARS-CoV-2 virus (M.O.I = 0.5) (n=3, 5-15 organoids per experiment). S and N (100

5   nM) were added to vascular organoids for 72 h in the presence and absence of IL-1β (20

6   ng/ml) (Peprotech) (n=5, 5-15 organoids per experiment).

7   **ELISA**

8   Soluble IL6 (IL6) (Peprotech) and IL8 (Peprotech) were measured in the supernatant of

9   untreated or treated organoids by ELISA. The levels of von Willebrand factor (VWF) were

10 measured using polyclonal antibodies against VWF (Agilent). Plasma-derived VWF

11 (Wilfactin) was used as a standard.

12 **qRT-PCR**

13 Whole organoids were processed using the Micro RNEasy Kit (Qiagen, Germany)

14 according to the manufacturer's instructions. Isolated RNA was quantified on the NanoDrop

15 ND-100 (Thermo Scientific, USA) and cDNA was prepared using 1 µg RNA using the High

16 Capacity cDNA Reverse Transcription Kit (Applied Biosystems, USA) according to the

17 manufacturer's instructions using standard cycling conditions. cDNA was then diluted to

18 5ng before being combined with PowerUp SYBR Green Master Mix reagent (Applied

19 Biosystems) and the relevant pre-designed PrimeTime IDT Primers. The absolute

20 expression of the respective genes was calculated using the ΔCt method using *GAPDH* as

21 an internal housekeeping control. Expression values were normalized to control conditions

22 and log transformed before plotting using GraphPad Prism 7.

23 **Organoids and Lung sections staining**

24 **Whole organoid staining.** Whole organoids from independent experiments were pooled,

25 fixed for 15 min in PFA 4 %, washed in phosphate buffer saline (PBS)-Tween-20 (PBS-T

26 0.05 %) and incubated overnight in blocking buffer (2 % goat serum, 1 % bovine serum

27 albumin (BSA)) supplemented with Triton-X100, and Sodium Deoxycholate. Samples were

28 then incubated overnight at 4 °C in blocking buffer containing primary antibodies

29 (Supplementary Table 2). Secondary Alexa Fluor antibodies (all from Invitrogen) were

30 added for 2 h, washed before staining with DAPI. Upon labelling, samples were washed

31 again in PBS-T, mounted in 0.5 % low melting point agarose (Fisher Scientific) in an Ibidi 8-

32 well slide (Ibidi). Samples were then subject to serial dehydration in ethanol (30%, 50%, 70

1 %, 100 %) before clearing in ethyl cinnamate and imaging using Airyscan confocal

2 microscopy.

3 **Organoid sections staining.** Vascular organoids from independent experiments were

4 fixed for 15 min in PFA 4 % and frozen in optimum cutting temperature (OCT) compound

5 (Tissue-Tek, The Netherlands). Sections (12 µm) were blocked with PBS containing 5 %

6 BSA and 10 % goat serum for 1h and autofluorescence was quenched using ammonium

7 chloride 50 mM for 20 min. Primary antibodies against ACE2 (ThermoFischer scientific) and

8 CD144 (ThermoFischer scientific), Spike glycoprotein (Sinopharma), CD140b (Sigma-

9 Aldrich), Ulex Europaeus Agglutinin I (UEA1), ACE2 (Thermofisher) and Biotinylated

10 (VECTOR Laboratories) were incubated overnight at 4 °C. Click-iT™ TUNEL Alexa Fluor™

11 647 Imaging Assay (ThermoFischer) was used to stain for apoptosis. Secondary antibodies

12 were incubated for 1h at room temperature. Anti-NG2 Alexa Fluor 488 was incubated for 1h

13 at RT (Supplementary Table 2). Slides are mounted using ProLong Gold Antifade Mountant

14 with DAPI (Life Technologies). Sections were imaged using Epi fluorescent microscopy or

15 Airyscan confocal microscope and analyzed using ZEN software and image J.

16 **Lung sections staining.** For paraffin sections, following rehydration and antigen retrieval,

17 lung sections were treated with H_2O_2 3 % for 15 min and blocked with PBS containing 5 %

18 bovine serum albumin and 10 % goat serum for 1 h. Antibodies against Neural/glial antigen

19 2 (NG2), spike glycoprotein, Intercellular Adhesion Molecule 1, CD144 (VE-cadherin), VWF,

20 platelet CD42b and fibrin (Supplementary Figure 2) were incubated overnight at 4 °C.

21 Secondary antibodies were added for 1 h at room temperature. Nuclei were stained using

22 DAPI. Lung autofluorescence was quenched using commercial kit (Vector laboratories) and

23 slides mounted using ProLong Gold Antifade Mountant (Life Technologies). Sections were

24 imaged using Epi fluorescent microscopy or Zeiss Axio Scan.Z1 microscope and analyzed

25 using ZEN software and image J.

26 **Flow cytometry**

27 Organoids were harvested and dissociated using 200 U/ml collagenase type-II

28 (Worthington) resuspended in HBSS solution (Sigma-Aldrich). For dissociation, cells were

29 first washed twice with PBS before resuspension in collagenase solution and incubation at

30 37 °C for two 3 min intervals, with brief trituration between each step. The cells were

31 blocked with PBS-FBS 10% for 20 min on ice. Dead/live cells were detected using

32 Live/Dead Fixable Aqua Dead Cell Stain (Thermofischer). Cells were stained with anti

1 CD144-PEcy7, anti podoplanin-FITC, anti CD140b-PE, anti CD31-APC-Cy7 (all from

2 Biolegend), anti ICAM-1-Biotin followed by Streptavidin PE-CF594 (BD), anti NG2-APC

3 (Bio-Techne Ltd) for 20 min on ice. Cells were fixed and acquired by flow cytometry (Cyan,

4 Beckman Coulter). Cell death is shown as the fraction of cells negative for Live/Dead

5 Fixable Aqua Dead Cell Stain (live cells) over total cells detected within the endothelial

6 fraction (CD31+), fibroblast (CD140b$^+$NG2$^-$) or pericytes (CD140b$^+$NG2$^+$) populations.

7 Endothelial cells were defined as CD31$^+$ and CD144$^+$ double positive cells. The CD140b

8 positive population contained both pericytes (CD140b$^+$ NG2$^+$) and fibroblasts (CD140b$^+$

9 NG2$^-$) as assessed by flow cytometry (Supplementary Figure 1). CD144 expression is

10 assessed on CD31$^+$ cells (Supplementary Figure 1). Podoplanin and ICAM-1 expression

11 are assessed on pericytes (CD140b$^+$ NG2$^+$) and fibroblasts (CD140b$^+$ NG2$^-$).

12 **Image analysis**

13 Image analysis was performed using Fiji [34]. For measures of VE-Cadherin in patient

14 samples, 8-10 images across different slides and sections from each patient were taken

15 and analyzed. Within each image, an ROI was drawn around a vessel and the mean

16 intensity of the channel of interest was measured and plotted. For co-localization studies,

17 ROIs were drawn around 5 distinct separate sectioned organoids and the Coloc2 method

18 was applied to find the Pearson's Correlation Co-efficient.

19 **Data analysis**

20 All data were presented as means ± standard deviation (s.d). The significant difference

21 groups were analyzed using either a One-Way ANOVA with multiple comparisons or a

22 Kruskal-Wallis Test with multiple comparisons as indicated in figure legends using Prism 7

23 (GraphPad Software Inc, USA).

24 **Results**

25 **Spike glycoprotein is detected in NG2$^+$-pericytes in autopsies of patients with COVID-**

26 **19 and is associated with decreased endothelial permeability and thrombosis**

27 In the presence of conflicting data supporting endothelial viral uptake and with evidence of

28 an emerging role of brain and heart pericytes in SARS-CoV-2 infection [19,20], we reasoned

29 that SARS-CoV-2 targets pericytes in the microvasculature of the lung in patients with

30 severe COVID-19, altering the crosstalk with endothelial cells and promoting vascular

1   permeability and damage. As a first step, we assessed the presence of the spike

2   glycoprotein in pericytes of lung tissues obtained *post mortem* from eight patients who died

3   from COVID-19 (Supplementary Table 1). Immunostaining analysis of the viral spike

4   glycoprotein revealed positive staining in NG2-positive (NG2$^+$) pericytes in 5 patients with

5   COVID-19 while it was undetectable in age-matched non-COVID19 control lung autopsies

6   (Figure 1A, B, C, Supplementary Figure 2). Notably, the presence of the spike glycoprotein

7   in the lungs and its colocalization with pericytes was heterogenous among patients (Figure

8   1B, Supplementary Figure 2). NG2$^+$ Spike$^+$ cells were not lining the endothelium, in

9   particular cells with high spike staining (as indicated in Figure 1B), and Spike signal was

10   associated with ICAM-1 staining (Figure 1A, C), suggesting pericyte activation and

11   detachment following infection.

12   Given that microvascular pericyte activation and apoptosis regulate microvascular

13   endothelial permeability [35], we assessed the expression of the endothelial junctional protein

14   VE-cadherin (CD144), as a marker for vascular permeability. In non-ventilated COVID-19

15   patients, CD144 expression on the microvascular vessels was decreased in SARS-CoV-2

16   infected lungs compared to control, most markedly in patients with confirmed macro and

17   micro-thrombosis (Figure 1D, E, Supplementary Figure 3). These results show that spike

18   glycoprotein strongly localizes with lung pericytes and this is associated with increased

19   pericyte detachment and a decrease in endothelial barrier function, in particular in patients

20   with thrombotic complications.

21   **Increased VWF and fibrin deposition in COVID-19 lungs patients with thrombotic**

22   **complications**

23   CD144 is crucial for endothelial stability and blockade of CD144 contributes to

24   coagulopathy, particularly in the lung microvasculature [36, 37]. We therefore assessed CD144

25   expression and markers of thrombosis in the lung autopsies of patients with COVID-19.

26   Diffuse alveolar damage with extensive hyaline membrane rich in fibrin was observed in all

27   patients (Figure 2A). Compared to lung autopsies from age-matched controls, we observed

28   a significant decrease in CD144 expression (Figure 1D, E, 2B-D, Supplementary Figure 3)

29   associated with platelet recruitment and VWF deposition in lung capillaries with low fibrin

30   content (Figure 2B-D, Supplementary Figure 4). Thrombi in the large vessels were rich in

31   VWF and fibrin, but with low content in platelets [38]. Megakaryocytes (CD42b$^+$) were also

1 observed in some patients (Figure 2C). VWF was significantly higher in patients with

2 thrombotic complications, supporting a key role for endothelial activation in thrombosis.

3 In order to assess whether CD144 downregulation is observed in other coronavirus family

4 member viruses, we also assessed the expression of CD144, platelets (CD42b$^+$) and fibrin

5 in lung autopsies from cases of Middle East respiratory syndrome coronavirus (MERS-CoV)

6 and rhinovirus. A decrease in CD144 expression and an increase in fibrin deposition and

7 platelet recruitment in the microvasculature was observed in MERS-CoV-infected lung

8 compared to control lung tissue (Figure 2E) whereas CD144 expression was more evident

9 in rhinovirus-infected lung without significant fibrin deposition or platelet recruitment (Figure

10 2F). These results suggest that in this small cohort of patients a decrease in CD144

11 expression and an increase in VWF deposition are observed in lung autopsies from patient

12 with COVID-19, in particular with documented thrombosis.

13 **Preferential SARS-CoV-2 uptake by pericytes in a vascular organoid model**

14 In order to assess the direct role of SARS-CoV-2 on pericytes and endothelial cells, we

15 generated 3D human vascular organoids [30, 31] (Figure 3A) comprised of vascular

16 endothelium (CD144$^+$), and pericytes (CD140b$^+$) (Figure 3B, Supplementary Figure 1). The

17 percentage of endothelial cells varies between 20-50% endothelial cells, 20-50% for

18 NG2$^+$CD140b$^+$ and 10-40% NG2$^-$CD140b$^+$. Co-staining of vascular organoid sections with

19 ACE2 and CD144 antibodies indicated a distribution of ACE2 outside the branching

20 junctions of endothelial cells (Figure 3C). ACE2 strongly colocalized with pericytes (NG2$^{+,}$

21 CD140b$^+$) with lower colocalization with the endothelial marker UAE1 (Figure 3D-F).

22 Organoids were then exposed to live SARS-CoV-2 virus (M.O.I 0.5) for 48 h and the

23 distribution of the spike glycoprotein assessed using immunofluorescence imaging (Figure

24 3G). Colocalization analysis showed a strong presence of the spike in CD140b/NG2$^+$

25 (Figure 3H) with lower levels detected in UAE1-positive endothelial cells (Figure 3H).

26 SARS-CoV-2 infection of vascular organoid was associated with increased cell apoptosis

27 as assessed using TUNEL staining (Figure 3I, J). TUNEL staining was observed in both

28 UAE1-positive endothelial cells and pericytes (CD140b/NG2$^+$), however it was significantly

29 higher in pericytes compared to endothelial cells (Figure 3K). SARS-CoV-2 infection

30 progressively altered the expression and distribution of NG2 within the infected organoids

31 associated with a decrease in CD144 expression (Figure 3L-N). The decrease in CD144

32 was not due to the loss of endothelial cells as shown using UAE1 staining (Supplementary

1 Figure 5). These results show that infection of vascular organoids with SARS-CoV-2

2 induces pericyte apoptosis and decreases CD144 expression through a preferential uptake

3 of the virus by pericytes. This is associated with a disruption of the vessel architecture,

4 detachment of pericytes and loss of vascular integrity.

5 **Spike glycoprotein and nucleocapsid protein impair endothelial integrity and survival**

6 **without significant activation**

7 In order to assess whether the spike glycoprotein is responsible for altered endothelial

8 integrity and cell survival, vascular organoids were treated with i) recombinant active

9 trimeric spike glycoprotein (S) (100 nM) [32, 39]; ii) nucleocapsid protein (N) (100 nM) [33] or iii) a

10 combination of both (S + N) for 72 h. Endothelial survival was assessed using live/dead

11 fixable dye staining, while endothelial cell activation and permeability was assessed using

12 ICAM-1 and CD144 expression, respectively (Supplementary Figure 1). Treatment of

13 vascular organoids with S, N or S+N decreased endothelial cell survival as assessed by a

14 decrease in the fraction of live endothelial cells from total cells (Figure 4A, B). Co-

15 stimulation with IL-1β, a potent pro-inflammatory cytokine, did not alter cell death compared

16 to viral antigen alone. Similar to SARS-CoV-2 infection, treatment of vascular organoids

17 with viral antigens decreased the number of endothelial cells (CD144$^+$/CD31$^+$ cells; Figure

18 4C). Treatment with viral antigens did not induce endothelial cell activation as assessed by

19 the expression of ICAM-1 on endothelial cells (Figure 4D). No significant change in the

20 levels of IL6, IL8 and VWF in the supernatants were observed following viral antigen

21 treatment compared to untreated organoids (Figure 4E, F, G). These results support a role

22 for N and S protein in regulating endothelial cell death and integrity without inducing

23 significant endothelial activation.

24 **Spike glycoprotein and nucleocapsid protein induce pericyte death in vascular**

25 **organoids**

26 We further assessed pericyte and fibroblast survival and activation following viral antigen

27 treatment by flow cytometry. Viral antigens N and S decreased pericyte survival as

28 assessed by a decrease in the live fraction of pericytes among total cells (Figure 4H, I).

29 Despite the presence of ICAM-1-positive pericytes in patient lung sections, no significant

30 activation of pericytes was observed in vascular organoids as measured by the expression

31 of ICAM-1 on CD140b$^+$NG2$^+$ pericytes (Figure 4J). Addition of IL-1β did not alter cell

32 survival or activation compared to antigen alone (Figure 4J). No significant cell death of

1   activation was observed in the fibroblast population (Supplementary Figure 6). These

2   results show that S and N antigens alter pericyte survival without inducing direct activation.

3   **Spike and N proteins alter gene expression linked to vascular integrity and**

4   **permeability in vascular organoids**

5   To investigate the mechanisms by which viral infection of the vasculature drives the loss of

6   CD144 expression, we treated vascular organoids with S and N for 4, 24 and 72 h hours to

7   assess transcriptional changes in key genes involved in the maintenance of vascular

8   barriers by qRT-PCR. These included genes encoding for angiopoietin-1 (*ANGPT1*),

9   angiopoietin-2 (*ANGPT2*), sphingosine kinase 1 (*SPHK1*), sphingosine kinase 2 (*SPHK2*),

10   Notch receptor 3 (*NOTCH3*), beta catenin 1 (*CTNNB1*), Jagged Canonical Notch Ligand 1

11   (*JAG1*), Jagged Canonical Notch Ligand 2 (*JAG2*), CD144 (*CDH5*), CD31 (*PECAM*), Tie2

12   (*TEK*), *ACE2*, *PDGFRB*, Toll like receptor 4 (*TLR4*), and Integrin alpha 4 (*ITGA4*).

13   Compared to untreated organoids, we found significant down-regulation in *NOTCH3*,

14   *SPHK2*, and *TEK*, while in contrast we saw a marked upregulation of *ACE2*, *ANGPT2* and

15   *SPHK1* (Figure 3K, Supplementary Figure 7). No significant changes in *CDH5*, *ANGPT1* or

16   other genes was observed. These results show that S and N treatments alter the

17   expression of gene regulating vascular integrity and permeability.

18   **Discussion**

19   In this study, we used lung autopsy sections from patients with COVID-19 and a 3D

20   vascular organoid model to show that SARS-CoV-2 and its antigens S and N decrease the

21   expression of the adhesion junction molecule CD144 and alter endothelial cell and pericyte

22   survival without inducing endothelial activation. We also observe a decrease in CD144

23   expression in the lung microvasculature of COVID-19 patients that is associated with

24   increased platelet recruitment and VWF deposition. The preferential uptake of SARS-CoV-2

25   by pericytes in the vascular organoid alters the expression of pericyte and endothelial

26   genes regulating endothelial permeability and integrity, increasing cell permeability and

27   death.

28   During homeostasis, the integrity of the vasculature is maintained through a tight crosstalk

29   between mural and endothelial cells. Pericytes and endothelial cells establish connections

30   to maintain endothelial quiescence through cell-cell contact via "Peg-and-socket" like

31   membrane structures which include tight (claudin, occludin and JAM-1), gap (connexin43)

32   and adherent (N-cadherin) junctions and through focal adhesion plaques allowing indirect

1   interactions between both cells via the extracellular matrix through integrins [40]. Pericyte and

2   endothelial cells can also communicate through paracrine signaling of growth factor

3   (angiopoetin-1 and PDGF), their receptors (Tie2 and PDGFRb) and juxtacrine signaling

4   (Jagged1-Notch3) [6]. Following inflammatory or infectious challenge, as observed during

5   severe SARS-CoV-2 infection, the protective effect of the endothelium is lost, promoting a

6   thrombotic and inflammatory microenvironment, supporting platelet recruitment, activation

7   of the coagulation cascade and thrombosis. Indeed, endotheliitis, endothelial dysfunction

8   and death are hallmarks of severe SARS-CoV-2 infection [1, 41]. Using a vascular organoid

9   model, we observed that SARS-CoV-2 or viral antigens S and N downregulate CD144

10   expression on endothelial cells, increasing cell death. CD144 mediates endothelial cell

11   interactions and antibodies blocking this interaction increase endothelial permeability,

12   apoptosis, vascular instability and hemorrhages [42, 43]. This can also expose the

13   prothrombotic extracellular matrix to blood cells, such as platelets, promoting a thrombotic

14   state [37]. The detection of spike glycoprotein in pericytes in vascular organoids and COVID-

15   19 lung autopsies suggests preferential uptake of SARS-CoV-2 by pericytes, probably due

16   to the high expression of ACE2, is a key contributor for pericyte and endothelial damage

17   [44,45]. This effect was mediated by pericyte infection, as the presence of the spike

18   glycoprotein was mainly observed in pericytes, both in vascular organoids and COVID-19

19   lung autopsies. The increase in apoptosis observed could be due to a reduction in the

20   capacity of infected pericytes to support an endothelial network. This, in turn, produces pro-

21   apoptotic factors resulting in EC death as recently shown using primary cardiac pericytes [22].

22   Using a cortical organoid model, pericytes were shown to serve as a replication site for

23   SARS-CoV-2 allowing viral production, transport and infection of other cells such as

24   astrocytes mediating their death [23]. In a model of vascular organoids, SARS-CoV-2

25   infection and replication was inhibited by human soluble recombinant ACE2, although the

26   cell type involved were not identified[29]. In this study, we identified the pericytes as the main

27   cells responsible for SARS-CoV-2 uptake within the vascular organoids. SARS-CoV-2

28   infection of pericytes in vascular organoids results in increased apoptosis in both pericytes

29   and endothelial cells, thereby increasing vascular permeability. Moreover, the loss of

30   pericytes increases endothelial cell sprouting and intussusceptive angiogenesis in SARS-

31   CoV-2-infected lungs combined with disruption of intercellular junctions, cell swelling and a

32   loss of contact with the basal membrane [5]. Despite a lower expression of ACE2 on

33   endothelial cells, SARS-CoV-2 can also directly impair endothelial permeability by acting

34   directly on endothelial cells[46]. The effect of spike protein mediated endothelial dysfunction

1   was further increased on diabetic endothelial cells, supporting a role for chronic disease-

2   induced vessel damage in the high susceptibility to cell damage. The effect of the spike is

3   not limited to CD144, as a significant decrease in the tight junction protein JAM-A and the

4   gap junction protein connexin-43 were also observed [46]. We did not observe an alteration in

5   the gene expression of CDH5, suggesting CD144 undergoes internalization and

6   degradation. Indeed, it was recently shown that the spike protein-induced internalization of

7   ACE2 triggered the subsequent internalization and degradation of key junction proteins

8   impairing endothelial barrier integrity [45].

9   In addition to the decrease in endothelial junction protein CD144, we observed that addition

10   of the spike and N proteins induced gene expression of angiopoietin-2 while downregulating

11   NOTCH3. These data are consistent with previous observations showing that knockdown of

12   NOTCH3 using siRNA increases proinflammatory genes including angiopoietin-2 and

13   ICAM-1, induces pericyte dysfunction and pericyte-endothelial cell interaction

14   destabilization promoting vascular leakage. Angiopoietin-2 is a non-signal transducing

15   ligand of Tie-2 produced by endothelial cells. Activation of the Tie-2 signaling pathway by

16   angoipoietin-2 destabilizing the vasculature by inhibiting the protecting effect of

17   angiopoietin-1. Moreover, angiopoietin-2 induces pericyte damage and detachment,

18   increasing vascular leakage and immune cell migration. This process increases

19   plasminogen activator inhibitor-1 (PAI-1) in endothelial cells, which supports coagulation,

20   endothelial activation and inflammation [47]. An increase in the levels of angiopoietin-2 [48] and

21   PAI-1 [49] is observed in patients with COVID-19 and associates with thrombo-embolic

22   events.

23   Pericyte activation and dysfunction increase EC procoagulant activity and endothelial

24   permeability, as constitutive hypoplasia of pericytes increases VWF release, tissue factor

25   expression and platelet adhesion. In this study, we did not observe a significant increase in

26   VWF in the supernatant of vascular organoids treated with viral antigens, suggesting that

27   VWF release associated with endothelial activation may result from the dysregulated

28   immune/inflammatory response associated with SARS-CoV-2 infection rather than pericyte

29   or endothelial cell infection [50-54]. With the lack of efficacy of anti-platelet drugs in improving

30   outcome in severe COVID-19 patients [38, 55, 56] endothelial activation and release of VWF

31   represents a potential target to limit thrombosis in COVID-19 patients. Recently, platelet

32   activation and secretion of S100 A8/A9, a damage-associated molecular pattern, was

33   shown to induce endothelial activation, supporting a role for platelet recruitment and

1　activation in endotheliitis [11]. These effects can be exacerbated by comorbidities, which can

2　increase endothelial and pericyte responses to infection. Further studies using vascular

3　organoid models mimicking disease state can shed light on the mechanisms of endothelial

4　activation during SARS-CoV-2 infection.

5　Our study has however some limitations. The detection of spike glycoprotein in lung

6　pericytes was heterogenous in our small cohort of lung autopsies. This could be due to

7　different infection rate and incubation time, patients' comorbidities or other unknown factors.

8　The infection of pericytes was shown using our vascular organoid model as well as a

9　cortical organoid model, supporting a key role for pericyte infection in altering the

10　communication with neighboring cells. Moreover, these observations need to be validated

11　in a larger number of lung autopsies, due to the limited sections available for this study.

12　In conclusion, we propose that direct infection of pericytes by SARS-CoV-2 induces

13　pericyte damage and dysregulates the crosstalk with endothelial cells, increasing vascular

14　permeability. However, endothelial activation is more likely regulated by the inflammatory

15　response and platelet recruitment and activation in particular in the microcirculation rather

16　than direct viral infection and combined endothelial activation and increased vascular

17　permeability promotes vasculopathies.

18

19　**Declarations**

20　**Funding**

32

1   **Author contributions**

2   Contribution: AOK and JR designed research, performed research, analyzed data and

3   wrote the paper; JSR performed research and analyzed data; JHB and MC contributed to

4   data analysis; MLN, JDA, MC, AF contributed vital new reagents; EY, PGM, GT, AGR

5   contributes to clinical information and samples collection; ZS, HH and MP contributed vital

6   new reagents, performed experiments and analyzed data; All authors read and approved

7   the paper.

8   **Conflict of interest**

9   The authors have no conflicts of interest to declare that are relevant to the content of this

10 article.

11 **Data availability**

12 Any relevant data is available on request.

13

14

References

1. Varga Z, Flammer AJ, Steiger P, Haberecker M, Andermatt R, Zinkernagel AS, Mehra MR, Schuepbach RA, Ruschitzka F, Moch H. Endothelial cell infection and endotheliitis in COVID-19. *Lancet* 2020;**395**:1417-1418.

2. Klok FA, Kruip M, van der Meer NJM, Arbous MS, Gommers D, Kant KM, Kaptein FHJ, van Paassen J, Stals MAM, Huisman MV, Endeman H. Incidence of thrombotic complications in critically ill ICU patients with COVID-19. *Thromb Res* 2020;**191**:145-147.

3. Rapkiewicz AV, Mai X, Carsons SE, Pittaluga S, Kleiner DE, Berger JS, Thomas S, Adler NM, Charytan DM, Gasmi B, Hochman JS, Reynolds HR. Megakaryocytes and platelet-fibrin thrombi characterize multi-organ thrombosis at autopsy in COVID-19: A case series. *EClinicalMedicine* 2020;**24**:100434.

4. Wichmann D, Sperhake JP, Lutgehetmann M, Steurer S, Edler C, Heinemann A, Heinrich F, Mushumba H, Kniep I, Schroder AS, Burdelski C, de Heer G, Nierhaus A, Frings D, Pfefferle S, Becker H, Bredereke-Wiedling H, de Weerth A, Paschen HR, Sheikhzadeh-Eggers S, Stang A, Schmiedel S, Bokemeyer C, Addo MM, Aepfelbacher M, Puschel K, Kluge S. Autopsy Findings and Venous Thromboembolism in Patients With COVID-19: A Prospective Cohort Study. *Ann Intern Med* 2020;**173**:268-277.

5. Ackermann M, Mentzer SJ, Jonigk D. Pulmonary Vascular Pathology in Covid-19. Reply. *N Engl J Med* 2020;**383**:888-889.

6. Armulik A, Abramsson A, Betsholtz C. Endothelial/pericyte interactions. *Circ Res* 2005;**97**:512-523.

7. Rayes J, Jadoui S, Lax S, Gros A, Wichaiyo S, Ollivier V, Denis CV, Ware J, Nieswandt B, Jandrot-Perrus M, Watson SP, Ho-Tin-Noe B. The contribution of platelet glycoprotein receptors to inflammatory bleeding prevention is stimulus and organ dependent. *Haematologica* 2018;**103**:e256-e258.

8. McCracken IR, Saginc G, He L, Huseynov A, Daniels A, Fletcher S, Peghaire C, Kalna V, Andaloussi-Mae M, Muhl L, Craig NM, Griffiths SJ, Haas JG, Tait-Burkard C, Lendahl U, Birdsey GM, Betsholtz C, Noseda M, Baker AH, Randi AM. Lack of Evidence of Angiotensin-Converting Enzyme 2 Expression and Replicative Infection by SARS-CoV-2 in Human Endothelial Cells. *Circulation* 2021;**143**:865-868.

9. Qian Y, Lei T, Patel PS, Lee CH, Monaghan-Nichols P, Xin HB, Qiu J, Fu M. Direct activation of endothelial cells by SARS-CoV-2 nucleocapsid protein is blocked by Simvastatin. *J Virol* 2021:JVI0139621.

10. Lei Y, Zhang J, Schiavon CR, He M, Chen L, Shen H, Zhang Y, Yin Q, Cho Y, Andrade L, Shadel GS, Hepokoski M, Lei T, Wang H, Zhang J, Yuan JX, Malhotra A, Manor U, Wang S, Yuan ZY, Shyy JY. SARS-CoV-2 Spike Protein Impairs Endothelial Function via Downregulation of ACE 2. *Circ Res* 2021;**128**:1323-1326.

11. Barrett TJ, Cornwell M, Myndzar K, Rolling CC, Xia Y, Drenkova K, Biebuyck A, Fields AT, Tawil M, Luttrell-Williams E, Yuriditsky E, Smith G, Cotzia P, Neal MD, Kornblith LZ, Pittaluga S, Rapkiewicz AV, Burgess HM, Mohr I, Stapleford KA, Voora D, Ruggles K, Hochman J, Berger JS. Platelets amplify endotheliopathy in COVID-19. *Sci Adv* 2021;**7**:eabh2434.

12. Hottz ED, Azevedo-Quintanilha IG, Palhinha L, Teixeira L, Barreto EA, Pao CRR, Righy C, Franco S, Souza TML, Kurtz P, Bozza FA, Bozza PT. Platelet activation and platelet-monocyte aggregate formation trigger tissue factor expression in patients with severe COVID-19. *Blood* 2020;**136**:1330-1341.

13. Connors JM, Levy JH. COVID-19 and its implications for thrombosis and anticoagulation. *Blood* 2020;**135**:2033-2040.

14. Borczuk AC, Salvatore SP, Seshan SV, Patel SS, Bussel JB, Mostyka M, Elsoukkary S, He B, Del Vecchio C, Fortarezza F, Pezzuto F, Navalesi P, Crisanti A, Fowkes ME, Bryce CH, Calabrese F, Beasley MB. COVID-19 pulmonary pathology: a multi-institutional autopsy cohort from Italy and New York City. *Mod Pathol* 2020;**33**:2156-2168.

15. Muus C, Luecken MD, Eraslan G, Sikkema L, Waghray A, Heimberg G, Kobayashi Y, Vaishnav ED, Subramanian A, Smillie C, Jagadeesh KA, Duong ET, Fiskin E, Triglia ET, Ansari M, Cai P, Lin B, Buchanan J, Chen S, Shu J, Haber AL, Chung H, Montoro DT, Adams T, Aliee H, Allon SJ, Andrusivova Z, Angelidis I, Ashenberg O, Bassler K, Becavin C, Benhar I, Bergenstrahle J, Bergenstrahle L, Bolt L, Braun E, Bui LT, Callori S, Chaffin M, Chichelnitskiy E, Chiou J, Conlon TM, Cuoco MS, Cuomo ASE, Deprez M, Duclos G, Fine D, Fischer DS, Ghazanfar S, Gillich A, Giotti B, Gould J, Guo M, Gutierrez AJ, Habermann AC, Harvey T, He P, Hou X, Hu L, Hu Y, Jaiswal A, Ji L, Jiang P, Kapellos TS, Kuo CS, Larsson L, Leney-Greene MA, Lim K, Litvinukova M, Ludwig LS, Lukassen S, Luo W, Maatz H, Madissoon E, Mamanova L, Manakongtreecheep K, Leroy S, Mayr CH, Mbano IM, McAdams AM, Nabhan AN, Nyquist SK, Penland L, Poirion OB, Poli S, Qi C, Queen R, Reichart D, Rosas I, Schupp JC, Shea CV, Shi X, Sinha R, Sit RV, Slowikowski K, Slyper M, Smith NP, Sountoulidis A, Strunz M, Sullivan TB, Sun D, Talavera-Lopez C, Tan P, Tantivit J, Travaglini KJ, Tucker NR, Vernon KA, Wadsworth MH, Waldman J, Wang X, Xu K, Yan W, Zhao W, Ziegler CGK, Consortium NL, Human Cell Atlas Lung Biological N. Single-cell meta-analysis of SARS-CoV-2 entry genes across tissues and demographics. *Nat Med* 2021;**27**:546-559.

16. Clausen TM, Sandoval DR, Spliid CB, Pihl J, Perrett HR, Painter CD, Narayanan A, Majowicz SA, Kwong EM, McVicar RN, Thacker BE, Glass CA, Yang Z, Torres JL, Golden GJ, Bartels PL, Porell RN, Garretson AF, Laubach L, Feldman J, Yin X, Pu Y, Hauser BM, Caradonna TM, Kellman BP, Martino C, Gordts P, Chanda SK, Schmidt AG, Godula K, Leibel SL, Jose J, Corbett KD, Ward AB, Carlin AF, Esko JD. SARS-CoV-2 Infection Depends on Cellular Heparan Sulfate and ACE2. *Cell* 2020;**183**:1043-1057 e1015.

17. Hou YJ, Okuda K, Edwards CE, Martinez DR, Asakura T, Dinnon KH, 3rd, Kato T, Lee RE, Yount BL, Mascenik TM, Chen G, Olivier KN, Ghio A, Tse LV, Leist SR, Gralinski LE, Schafer A, Dang H, Gilmore R, Nakano S, Sun L, Fulcher ML, Livraghi-Butrico A, Nicely NI, Cameron M, Cameron C, Kelvin DJ, de Silva A, Margolis DM, Markmann A, Bartelt L, Zumwalt R, Martinez FJ, Salvatore SP, Borczuk A, Tata PR, Sontake V, Kimple A, Jaspers I, O'Neal WK, Randell SH, Boucher RC, Baric RS. SARS-CoV-2 Reverse Genetics Reveals a Variable Infection Gradient in the Respiratory Tract. *Cell* 2020;**182**:429-446 e414.

18. Bernard I, Limonta D, Mahal LK, Hobman TC. Endothelium Infection and Dysregulation by SARS-CoV-2: Evidence and Caveats in COVID-19. *Viruses* 2020;**13**.

19. Chen R, Wang K, Yu J, Howard D, French L, Chen Z, Wen C, Xu Z. The Spatial and Cell-Type Distribution of SARS-CoV-2 Receptor ACE2 in the Human and Mouse Brains. *Front Neurol* 2020;**11**:573095.

20. Chen L, Li X, Chen M, Feng Y, Xiong C. The ACE2 expression in human heart indicates new potential mechanism of heart injury among patients infected with SARS-CoV-2. *Cardiovasc Res* 2020;**116**:1097-1100.

21. Wong DWL, Klinkhammer BM, Djudjaj S, Villwock S, Timm MC, Buhl EM, Wucherpfennig S, Cacchi C, Braunschweig T, Knuchel-Clarke R, Jonigk D, Werlein C, Bulow RD, Dahl E, von Stillfried S, Boor P. Multisystemic Cellular Tropism of SARS-CoV-2 in Autopsies of COVID-19 Patients. *Cells* 2021;**10**.

22. Avolio E, Carrabba M, Milligan R, Kavanagh Williamson M, Beltrami AP, Gupta K, Elvers KT, Gamez M, Foster RR, Gillespie K, Hamilton F, Arnold D, Berger I, Davidson AD, Hill D, Caputo

M, Madeddu P. The SARS-CoV-2 Spike protein disrupts human cardiac pericytes function through CD147 receptor-mediated signalling: a potential non-infective mechanism of COVID-19 microvascular disease. *Clin Sci (Lond)* 2021;**135**:2667-2689.

23. Wang L, Sievert D, Clark AE, Lee S, Federman H, Gastfriend BD, Shusta EV, Palecek SP, Carlin AF, Gleeson JG. A human three-dimensional neural-perivascular 'assembloid' promotes astrocytic development and enables modeling of SARS-CoV-2 neuropathology. *Nat Med* 2021;**27**:1600-1606.

24. Stark K, Eckart A, Haidari S, Tirniceriu A, Lorenz M, von Bruhl ML, Gartner F, Khandoga AG, Legate KR, Pless R, Hepper I, Lauber K, Walzog B, Massberg S. Capillary and arteriolar pericytes attract innate leukocytes exiting through venules and 'instruct' them with pattern-recognition and motility programs. *Nat Immunol* 2013;**14**:41-51.

25. Teuwen LA, Geldhof V, Pasut A, Carmeliet P. COVID-19: the vasculature unleashed. *Nat Rev Immunol* 2020;**20**:389-391.

26. Delorey TM, Ziegler CGK, Heimberg G, Normand R, Yang Y, Segerstolpe A, Abbondanza D, Fleming SJ, Subramanian A, Montoro DT, Jagadeesh KA, Dey KK, Sen P, Slyper M, Pita-Juarez YH, Phillips D, Bloom-Ackerman Z, Barkas N, Ganna A, Gomez J, Normandin E, Naderi P, Popov YV, Raju SS, Niezen S, Tsai LT, Siddle KJ, Sud M, Tran VM, Vellarikkal SK, Amir-Zilberstein L, Atri DS, Beechem J, Brook OR, Chen J, Divakar P, Dorceus P, Engreitz JM, Essene A, Fitzgerald DM, Fropf R, Gazal S, Gould J, Grzyb J, Harvey T, Hecht J, Hether T, Jane-Valbuena J, Leney-Greene M, Ma H, McCabe C, McLoughlin DE, Miller EM, Muus C, Niemi M, Padera R, Pan L, Pant D, Pe'er C, Pfiffner-Borges J, Pinto CJ, Plaisted J, Reeves J, Ross M, Rudy M, Rueckert EH, Siciliano M, Sturm A, Todres E, Waghray A, Warren S, Zhang S, Zollinger DR, Cosimi L, Gupta RM, Hacohen N, Hide W, Price AL, Rajagopal J, Tata PR, Riedel S, Szabo G, Tickle TL, Hung D, Sabeti PC, Novak R, Rogers R, Ingber DE, Gordon Jiang Z, Juric D, Babadi M, Farhi SL, Stone JR, Vlachos IS, Solomon IH, Ashenberg O, Porter CBM, Li B, Shalek AK, Villani AC, Rozenblatt-Rosen O, Regev A. A single-cell and spatial atlas of autopsy tissues reveals pathology and cellular targets of SARS-CoV-2. *bioRxiv* 2021.

27. Guo J, Wei X, Li Q, Li L, Yang Z, Shi Y, Qin Y, Zhang X, Wang X, Zhi X, Meng D. Single-cell RNA analysis on ACE2 expression provides insights into SARS-CoV-2 potential entry into the bloodstream and heart injury. *J Cell Physiol* 2020;**235**:9884-9894.

28. Meiners S, Eickelberg O, Konigshoff M. Hallmarks of the ageing lung. *Eur Respir J* 2015;**45**:807-827.

29. Monteil V, Kwon H, Prado P, Hagelkruys A, Wimmer RA, Stahl M, Leopoldi A, Garreta E, Hurtado Del Pozo C, Prosper F, Romero JP, Wirnsberger G, Zhang H, Slutsky AS, Conder R, Montserrat N, Mirazimi A, Penninger JM. Inhibition of SARS-CoV-2 Infections in Engineered Human Tissues Using Clinical-Grade Soluble Human ACE2. *Cell* 2020;**181**:905-913 e907.

30. Khan AO, Slater A, Maclachlan A, Nicolson PLR, Pike JA, Reyat JS, Yule J, Stapley R, Rayes J, Thomas SG, Morgan NV. Post-translational polymodification of beta1-tubulin regulates motor protein localisation in platelet production and function. *Haematologica* 2020;**Online ahead of print**.

31. Wimmer RA, Leopoldi A, Aichinger M, Kerjaschki D, Penninger JM. Generation of blood vessel organoids from human pluripotent stem cells. *Nat Protoc* 2019;**14**:3082-3100.

32. Watanabe Y, Allen JD, Wrapp D, McLellan JS, Crispin M. Site-specific glycan analysis of the SARS-CoV-2 spike. *Science* 2020;**369**:330-333.

33. Faustini SE, Jossi SE, Perez-Toledo M, Shields A, Allen JD, Watanabe Y, Newby ML, Cook A, Willcox CR, Salim M, Goodall M, Heaney JL, Marcial-Juarez E, Morley GL, Torlinska B, Wraith DC, Veenith T, Harding S, Jolles S, Mark PJ, Plant T, Huissoon A, O'Shea MK, Willcox BE,

Drayson MT, Crispin M, Cunningham AF, Richter AG. Detection of antibodies to the SARS-CoV-2 spike glycoprotein in both serum and saliva enhances detection of infection. *medRxiv* 2020.

34. Schindelin J, Arganda-Carreras I, Frise E, Kaynig V, Longair M, Pietzsch T, Preibisch S, Rueden C, Saalfeld S, Schmid B, Tinevez JY, White DJ, Hartenstein V, Eliceiri K, Tomancak P, Cardona A. Fiji: an open-source platform for biological-image analysis. *Nat Methods* 2012;**9**:676-682.

35. Kato K, Dieguez-Hurtado R, Park DY, Hong SP, Kato-Azuma S, Adams S, Stehling M, Trappmann B, Wrana JL, Koh GY, Adams RH. Pulmonary pericytes regulate lung morphogenesis. *Nat Commun* 2018;**9**:2448.

36. Duong CN, Nottebaum AF, Butz S, Volkery S, Zeuschner D, Stehling M, Vestweber D. Interference With ESAM (Endothelial Cell-Selective Adhesion Molecule) Plus Vascular Endothelial-Cadherin Causes Immediate Lethality and Lung-Specific Blood Coagulation. *Arterioscler Thromb Vasc Biol* 2020;**40**:378-393.

37. Corada M, Mariotti M, Thurston G, Smith K, Kunkel R, Brockhaus M, Lampugnani MG, Martin-Padura I, Stoppacciaro A, Ruco L, McDonald DM, Ward PA, Dejana E. Vascular endothelial-cadherin is an important determinant of microvascular integrity in vivo. *Proc Natl Acad Sci U S A* 1999;**96**:9815-9820.

38. Schrottmaier WC, Pirabe A, Pereyra D, Heber S, Hackl H, Schmuckenschlager A, Brunnthaler L, Santol J, Kammerer K, Oosterlee J, Pawelka E, Treiber SM, Khan AO, Pugh M, Traugott MT, Schorgenhofer C, Seitz T, Karolyi M, Jilma B, Rayes J, Zoufaly A, Assinger A. Adverse Outcome in COVID-19 Is Associated With an Aggravating Hypo-Responsive Platelet Phenotype. *Front Cardiovasc Med* 2021;**8**:795624.

39. Hsieh CL, Goldsmith JA, Schaub JM, DiVenere AM, Kuo HC, Javanmardi K, Le KC, Wrapp D, Lee AG, Liu Y, Chou CW, Byrne PO, Hjorth CK, Johnson NV, Ludes-Meyers J, Nguyen AW, Park J, Wang N, Amengor D, Lavinder JJ, Ippolito GC, Maynard JA, Finkelstein IJ, McLellan JS. Structure-based design of prefusion-stabilized SARS-CoV-2 spikes. *Science* 2020;**369**:1501-1505.

40. Duong CN, Vestweber D. Mechanisms Ensuring Endothelial Junction Integrity Beyond VE-Cadherin. *Front Physiol* 2020;**11**:519.

41. Jin Y, Ji W, Yang H, Chen S, Zhang W, Duan G. Endothelial activation and dysfunction in COVID-19: from basic mechanisms to potential therapeutic approaches. *Signal Transduct Target Ther* 2020;**5**:293.

42. Corada M, Liao F, Lindgren M, Lampugnani MG, Breviario F, Frank R, Muller WA, Hicklin DJ, Bohlen P, Dejana E. Monoclonal antibodies directed to different regions of vascular endothelial cadherin extracellular domain affect adhesion and clustering of the protein and modulate endothelial permeability. *Blood* 2001;**97**:1679-1684.

43. Dejana E, Orsenigo F, Lampugnani MG. The role of adherens junctions and VE-cadherin in the control of vascular permeability. *J Cell Sci* 2008;**121**:2115-2122.

44. Cardot-Leccia N, Hubiche T, Dellamonica J, Burel-Vandenbos F, Passeron T. Pericyte alteration sheds light on micro-vasculopathy in COVID-19 infection. *Intensive Care Med* 2020;**46**:1777-1778.

45. Raghavan S, Kenchappa DB, Leo MD. SARS-CoV-2 Spike Protein Induces Degradation of Junctional Proteins That Maintain Endothelial Barrier Integrity. *Front Cardiovasc Med* 2021;**8**:687783.

46. Rauti R, Shahoha M, Leichtmann-Bardoogo Y, Nasser R, Paz E, Tamir R, Miller V, Babich T, Shaked K, Ehrlich A, Ioannidis K, Nahmias Y, Sharan R, Ashery U, Maoz BM. Effect of SARS-CoV-2 proteins on vascular permeability. *Elife* 2021;**10**.

47. Akwii RG, Sajib MS, Zahra FT, Mikelis CM. Role of Angiopoietin-2 in Vascular Physiology and Pathophysiology. *Cells* 2019;**8**.

48. Smadja DM, Guerin CL, Chocron R, Yatim N, Boussier J, Gendron N, Khider L, Hadjadj J, Goudot G, Debuc B, Juvin P, Hauw-Berlemont C, Augy JL, Peron N, Messas E, Planquette B, Sanchez O, Charbit B, Gaussem P, Duffy D, Terrier B, Mirault T, Diehl JL. Angiopoietin-2 as a marker of endothelial activation is a good predictor factor for intensive care unit admission of COVID-19 patients. *Angiogenesis* 2020;**23**:611-620.

49. Zuo Y, Warnock M, Harbaugh A, Yalavarthi S, Gockman K, Zuo M, Madison JA, Knight JS, Kanthi Y, Lawrence DA. Plasma tissue plasminogen activator and plasminogen activator inhibitor-1 in hospitalized COVID-19 patients. *Sci Rep* 2021;**11**:1580.

50. Rauch A, Dupont A, Goutay J, Caplan M, Staessens S, Moussa M, Jeanpierre E, Corseaux D, Lefevre G, Lassalle F, Faure K, Lambert M, Duhamel A, Labreuche J, Garrigue D, De Meyer SF, Staels B, Van Belle E, Vincent F, Kipnis E, Lenting PJ, Poissy J, Susen S, Lille CRN, Members of the LSC. Endotheliopathy Is Induced by Plasma From Critically Ill Patients and Associated With Organ Failure in Severe COVID-19. *Circulation* 2020;**142**:1881-1884.

51. Goshua G, Pine AB, Meizlish ML, Chang CH, Zhang H, Bahel P, Baluha A, Bar N, Bona RD, Burns AJ, Dela Cruz CS, Dumont A, Halene S, Hwa J, Koff J, Menninger H, Neparidze N, Price C, Siner JM, Tormey C, Rinder HM, Chun HJ, Lee AI. Endotheliopathy in COVID-19-associated coagulopathy: evidence from a single-centre, cross-sectional study. *Lancet Haematol* 2020;**7**:e575-e582.

52. Philippe A, Chocron R, Gendron N, Bory O, Beauvais A, Peron N, Khider L, Guerin CL, Goudot G, Levasseur F, Peronino C, Duchemin J, Brichet J, Sourdeau E, Desvard F, Bertil S, Pene F, Cheurfa C, Szwebel TA, Planquette B, Rivet N, Jourdi G, Hauw-Berlemont C, Hermann B, Gaussem P, Mirault T, Terrier B, Sanchez O, Diehl JL, Fontenay M, Smadja DM. Circulating Von Willebrand factor and high molecular weight multimers as markers of endothelial injury predict COVID-19 in-hospital mortality. *Angiogenesis* 2021.

53. Cugno M, Meroni PL, Gualtierotti R, Griffini S, Grovetti E, Torri A, Lonati P, Grossi C, Borghi MO, Novembrino C, Boscolo M, Uceda Renteria SC, Valenti L, Lamorte G, Manunta M, Prati D, Pesenti A, Blasi F, Costantino G, Gori A, Bandera A, Tedesco F, Peyvandi F. Complement activation and endothelial perturbation parallel COVID-19 severity and activity. *J Autoimmun* 2021;**116**:102560.

54. Dupont A, Rauch A, Staessens S, Moussa M, Rosa M, Corseaux D, Jeanpierre E, Goutay J, Caplan M, Varlet P, Lefevre G, Lassalle F, Bauters A, Faure K, Lambert M, Duhamel A, Labreuche J, Garrigue D, De Meyer SF, Staels B, Vincent F, Rousse N, Kipnis E, Lenting P, Poissy J, Susen S, Lille Covid Research N. Vascular Endothelial Damage in the Pathogenesis of Organ Injury in Severe COVID-19. *Arterioscler Thromb Vasc Biol* 2021;**41**:1760-1773.

55. Berger JS, Kornblith LZ, Gong MN, Reynolds HR, Cushman M, Cheng Y, McVerry BJ, Kim KS, Lopes RD, Atassi B, Berry S, Bochicchio G, de Oliveira Antunes M, Farkouh ME, Greenstein Y, Hade EM, Hudock K, Hyzy R, Khatri P, Kindzelski A, Kirwan BA, Baumann Kreuziger L, Lawler PR, Leifer E, Lopez-Sendon Moreno J, Lopez-Sendon J, Luther JF, Nigro Maia L, Quigley J, Sherwin R, Wahid L, Wilson J, Hochman JS, Neal MD, Investigators AC-a. Effect of P2Y12 Inhibitors on Survival Free of Organ Support Among Non-Critically Ill Hospitalized Patients With COVID-19: A Randomized Clinical Trial. *JAMA* 2022;**327**:227-236.

56. Group RC. Aspirin in patients admitted to hospital with COVID-19 (RECOVERY): a randomised, controlled, open-label, platform trial. *Lancet* 2022;**399**:143-151.

1 **Figure 1: Detection of the spike glycoprotein in lung pericytes and decreased CD144**

2 **expression in COVID-19 patients.** (A) Immunofluorescence imaging of NG2⁺, spike

3 glycoprotein and ICAM-1 in formalin fixed and paraffin embedded lung from patient who

4 died from COVID-19 and control COVID-19⁻ (Control) lung sections. (B) High magnification

5 of immunofluorescence imaging of NG2⁺ and spike glycoprotein in lung section. Yellow

6 arrows indicating NG2⁺ cells without Spike glycoprotein lining vessels, while red arrows

7 indicate infected cells. (C) Quantification of ICAM-1 expression using ImageJ in lung

8 autopsies from two patients who died from non-respiratory-associated diseases, 4 COVID-

9 19 patients without thrombosis and 4 patients with detectable thrombosis (3-6 areas per

10 slide). (D) Representative immunofluorescence imaging of CD144 (VE-cadherin) in lung

11 sections. (E) Quantification of CD144 levels using ImageJ. One-Way ANOVA with multiple

12 comparisons performed for each statistical test with significance at (*** $p = < 0.001$).

13 **Figure 2: Decreased CD144 expression is associated with increased VWF deposition**

14 **in the lung of patients with COVID-19.** (A) H&E staining of lung sections from patients

15 who died from COVID-19 with or without evidence of thrombosis. (B, C)

16 Immunofluorescence imaging of CD144, VWF, platelets (CD42b) and fibrin in formalin-fixed

17 and paraffin-embedded lung sections. (D) Quantification of VWF in lung sections. (E, F)

18 Staining of CD144, CD42b, fibrin and DAPI in lung sections from patients infected with (E)

19 MERS-CoV and (F) Rhinovirus. Images were captured using a Zeiss Observer 7

20 Epifluorescence microscope and slide scanner Axio Scan Z1. (Kruskal Wallis Test

21 performed on a total of 3-5 lung sections from 3 control patients, 3 COVID-19 patients with

22 thrombosis and 3 without evidences of thrombosis (* $p = < 0.05$, ** $p = < 0.01$, *** $p = <$
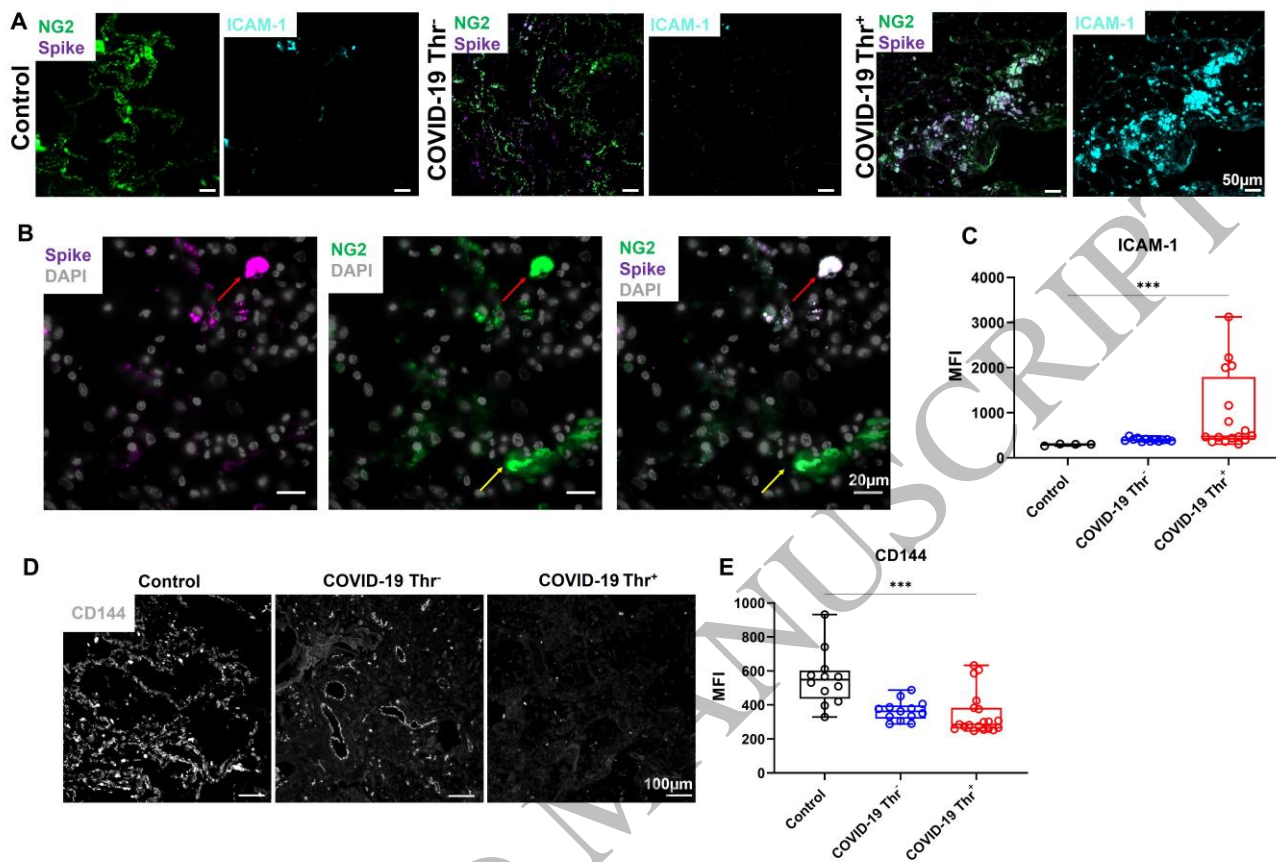
23 0.001, **** $p = < 0.0001$).

24 **Figure 3: Pericyte preferential uptake of SARS-CoV-2 increases vascular permeability**

25 **and endothelial and pericyte death in vascular organoids.** (A) Vascular organoids were

26 generated using a step wise differentiation of human induced pluripotent stem cells. (B) Cell

27 composition and distribution in mature vascular organoids were assessed using

28 immunofluorescence whole mount microscopy. (C) Immunofluorescence imaging of ACE2

29 and CD144 positive cells in organoids (12 µm organoid sections. (D) Sections of vascular

30 organoids were co-stained for pericytes (NG2) and ACE2. (E) Staining for UAE-1, ACE2,

31 CD140b and DAPI in vascular organoids. (F) Co-localization analysis between ACE2 and

32 CD140b compared ACE2 co-localization with UAE1 as measured by the Pearson's

33 Correlation Co-Efficient. (G) Co-staining for the spike glycoprotein in endothelial organoids

34 with CD140b⁺ cells treated with SARS-CoV-2. (H) Quantification of co-localization of the

1 spike glycoprotein between endothelium and pericytes. (I) Sections of vascular organoids

2 were stained with apoptosis marker TUNEL and nuclei staining DAPI. (J) Quantification of

3 TUNEL staining in control and SARS-CoV-2 treated vascular organoids. (K) Co-localization

4 of the TUNEL staining with UAE-1 (endothelium)and pericyte (CD140b$^+$). (L) Staining of

5 control and SARS-CoV-2 infected organoids for CD144, pericytes (NG2) and nuclei (DAPI).

6 (M) Immunofluorescence imaging of CD144 and nuclei (DAPI) in whole vascular organoids

7 treated with SARS-CoV-2 (M.O.I= 0.5) for 48 h. (N) Quantification of CD144 staining in

8 control and SARS-CoV-2 treated vascular organoids. (O) Staining for NG2, UAE-1, TUNEL,

9 and spike in control and SARS-CoV-2 infected organoids (48h). N = 4 for organoids

10 experiments, where one replicate is a total of 8-10 individual organoids pooled for assays

11 from each of 4 independent biological replicates. Each biological repeat was a separate

12 differentiation protocol followed by viral infection. For co-localizations un-paired T-Tests

13 were performed (** p = < 0.01) Schematic created on Biorender.com.

14 **Figure 4: Recombinant viral antigens S and N increase vascular permeability and**
15 **death without endothelial activation.** (A-D) Vascular organoids were treated with spike
16 glycoprotein (S) (100 nM), nucleocapsid (N) or a combination of both proteins for 72 h in the
17 presence or absence of IL1-β (20 ng/ml) compared to control was measured by flow
18 cytometry. (A) Representative flow cytometry blots of endothelial cell treated with S, N, and
19 S and N antigens in the presence and absence of IL1-β. (B) Fold change in the live
20 population of CD31$^+$ cells from the total population using Live/Dead fixable dead cell stain.
21 (C) Fold change in CD144 expression on CD31$^+$cells compared to untreated organoids and
22 (D) fold change in ICAM-1 expression on CD31$^+$ cells in treated organoids versus untreated
23 were measured by flow cytometry. (E) Detection of the levels of soluble IL6, (F) IL8 and (G)
24 VWF in the supernatant of organoids treated for 72 h with viral antigens in the presence or
25 absence of IL-1β by ELISA (n=3 independent experiments, 3-4 replicate per experiment).
26 (H) Representative flow cytometry plots of pericytes treated with S, N, and S and N
27 antigens in the presence and absence of IL1-β (20 ng/ml). (I) Live/dead NG2$^+$ cells from the
28 total population, (J) fold change in ICAM-1 expression on CD140$^+$NG2$^+$ cells in treated
29 organoids versus untreated were measured by flow cytometry. (K) qPCR of vascular
30 organoids treated with combination S and N proteins for 0, 4, 24 and 72 h for genes
31 regulating endothelial permeability. N = 3 for experiments, where one replicate is a total of
32 12-15 individual organoids pooled for assays from each of 3 independent biological
33 replicates (independent differentiations). One-Way ANOVA with multiple comparisons
34 performed for each statistical test with significance at (* p = < 0.05, ** p = < 0.01, *** p = <
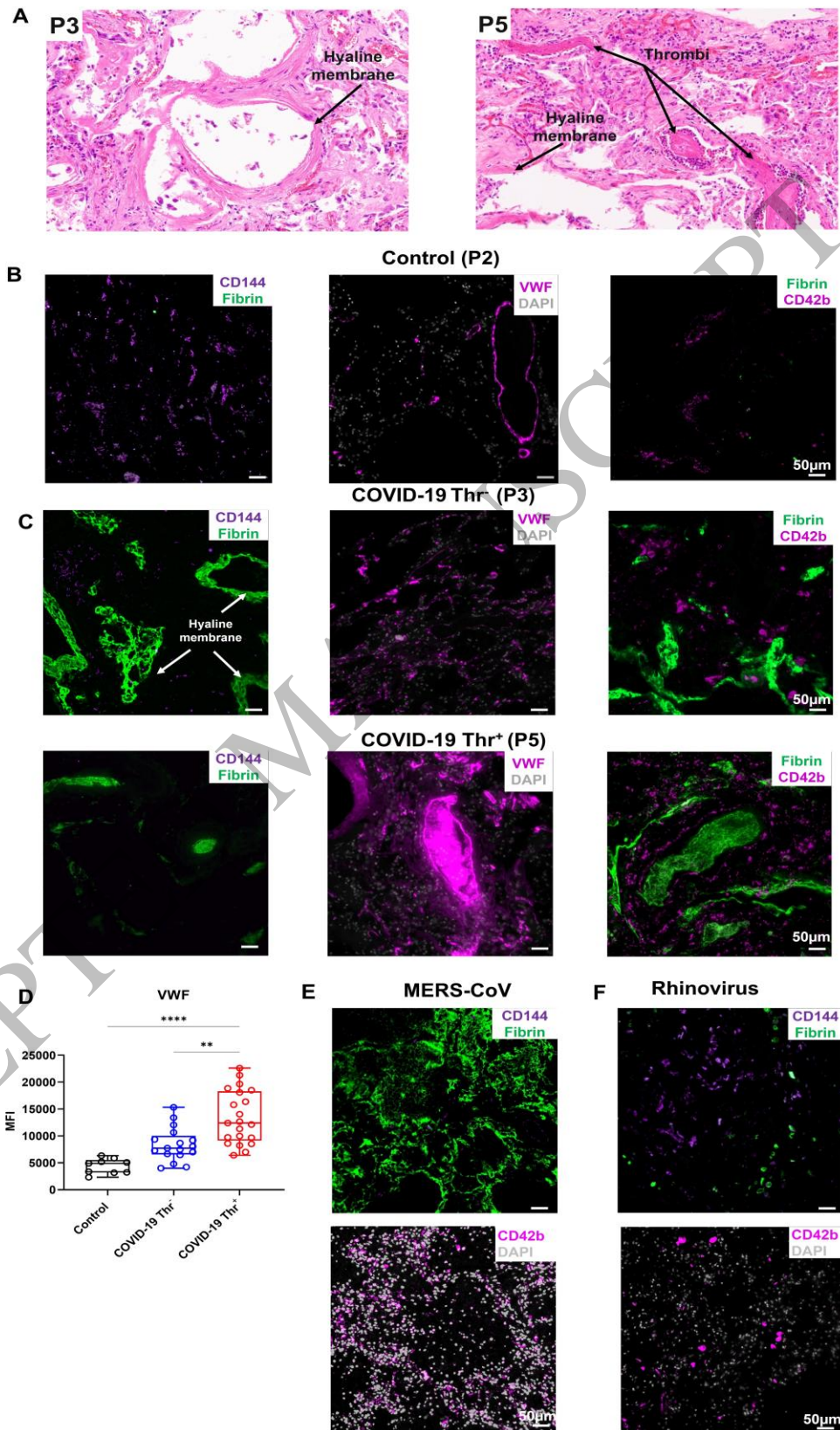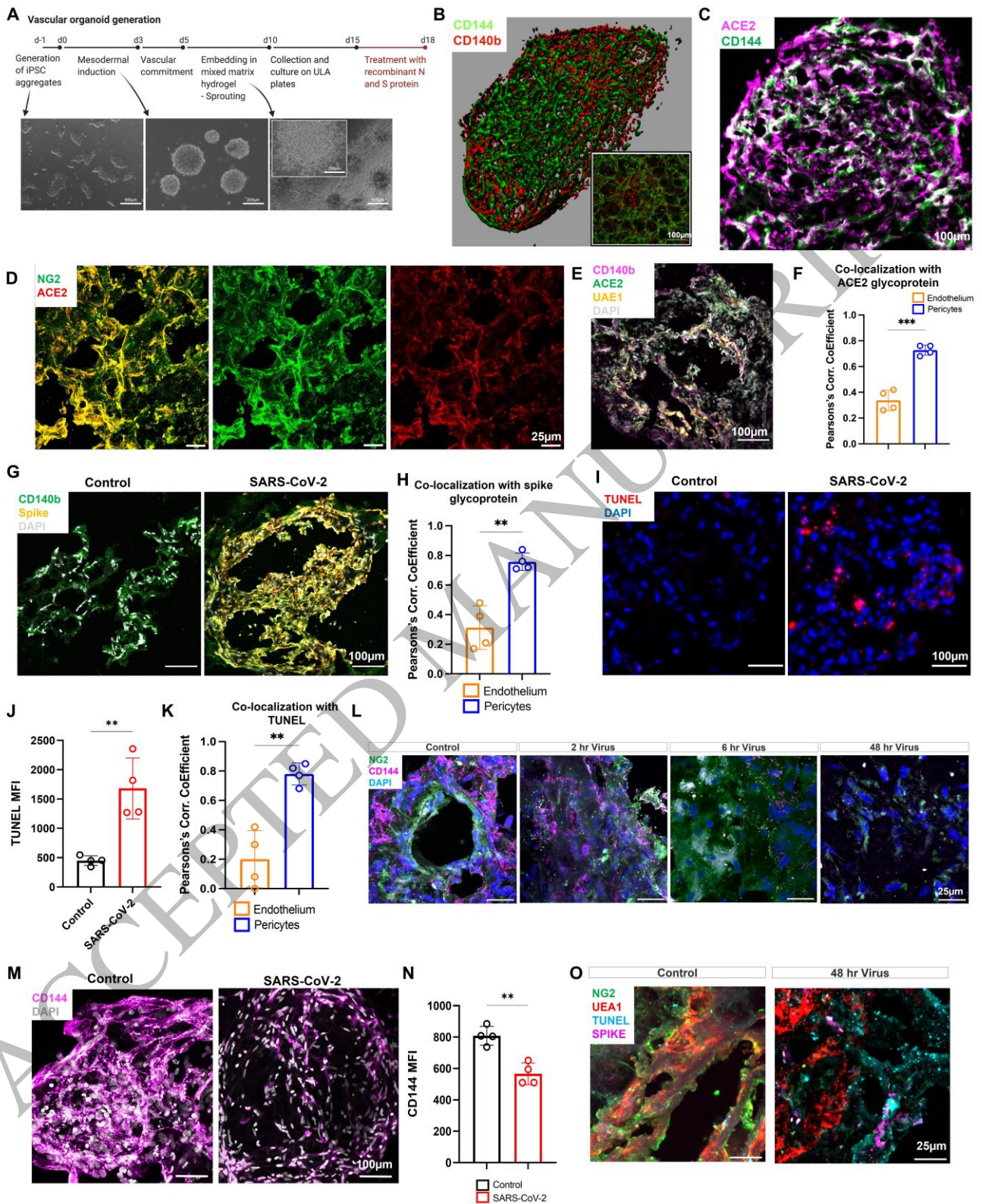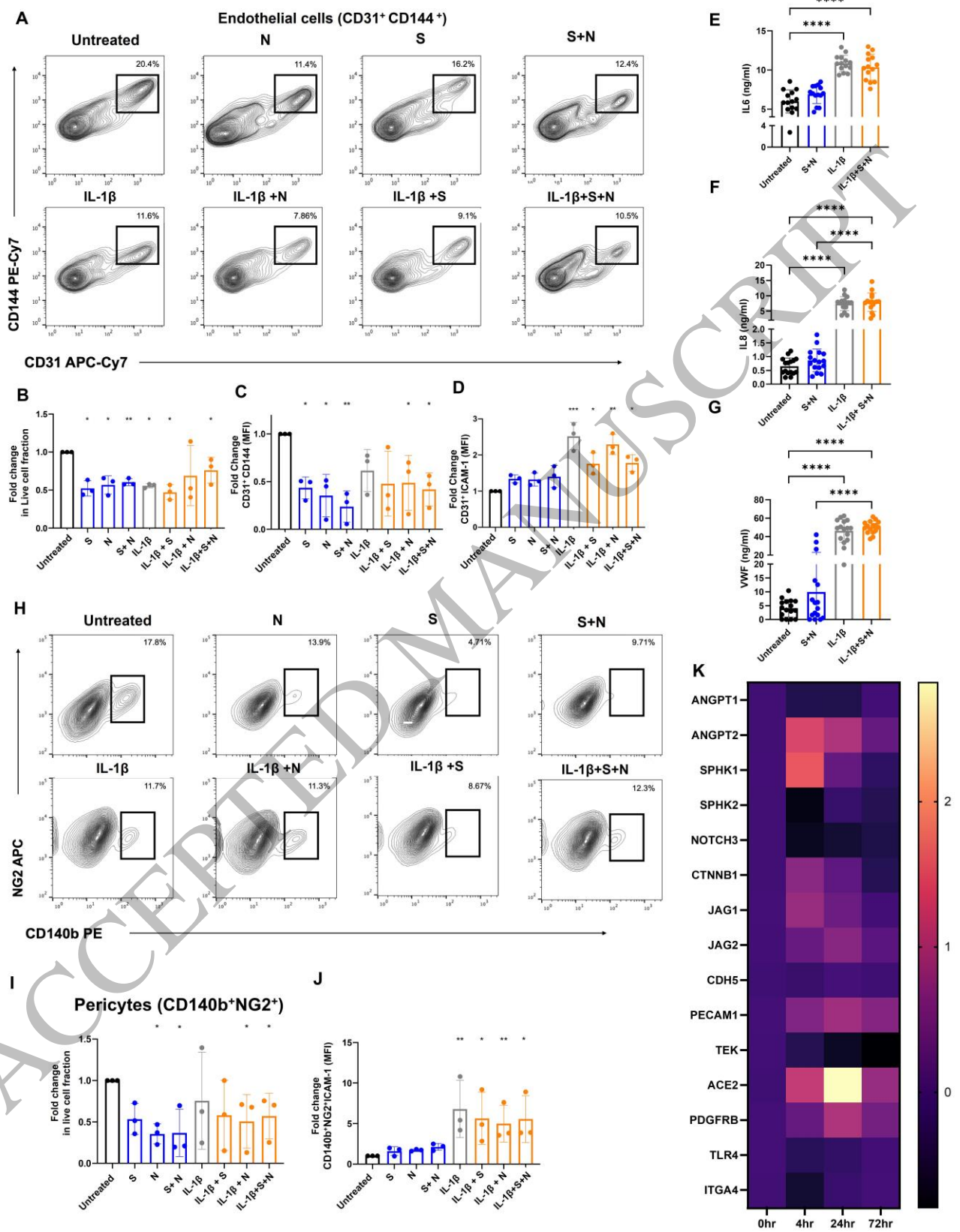35 0.001, **** p = < 0.0001).

36

37

Figure 1

1

2

Figure 2

Figure 3

27

Figure 4